Article (refereed) - postprint

Vogel, Christian; Sekine, Ryo; Steckenmesser, Daniel; Lombi, Enzo; Herzel, Hannes; Zuin, Lucia; Wang, Dongniu; Félix, Roberto; Adam, Christian. 2019. **Combining diffusive gradients in thin films (DGT) and spectroscopic techniques for the determination of phosphorus species in soils**.

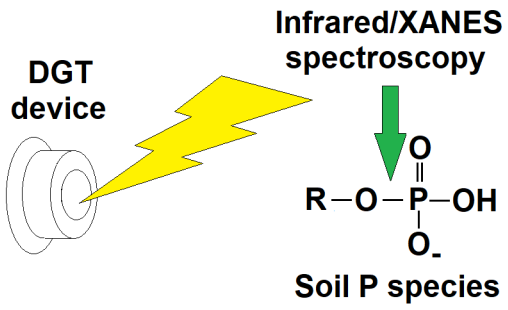

Combining Diffusive Gradients in Thin films (DGT) and Spectroscopic Techniques for the Determination of Phosphorus Species in Soils

Christian Vogel[1], Ryo Sekine[2,3], Daniel Steckenmesser[4], Enzo Lombi[3], Hannes Herzel[1], Lucia Zuin[5], Dongniu Wang[5], Roberto Félix[6] and Christian Adam[1]*

[1] Division 4.4 Thermochemical Residues Treatment and Resource Recovery, Bundesanstalt für Materialforschung und –prüfung (BAM), Unter den Eichen 87, 12205 Berlin, Germany

[2] Centre for Ecology & Hydrology, Maclean Building, Benson Lane, Crowmarsh Gifford, Wallingford, Oxfordshire OX10 8BB, United Kingdom

[3] Future Industries Institute, University of South Australia, Building X, Mawson Lakes, SA 5095, Australia

[4] Institute of Plant Nutrition, Research Center for Biosystems, Land Use and Nutrition, Justus-Liebig University Giessen, Heinrich-Buff-Ring 26-32, 35392 Giessen, Germany

[5] Canadian Light Source, 44 Innovation Boulevard, Saskatoon, SK S7N 2V3, Canada

[6] Renewable Energy, Helmholtz-Zentrum Berlin für Materialien und Energie GmbH, Hahn-Meitner-Platz 1, 14109 Berlin, Germany

* Corresponding author: e-mail: cv.vogel@yahoo.de

Keywords:

Phosphorus plant-availability, X-ray adsorption near-edge structure (XANES) spectroscopy, infrared spectroscopy, Diffusive Gradients in Thin films (DGT)

Abstract:

A wide range of methods are used to estimate the plant-availability of soil phosphorus (P). Published research has shown that the diffusive gradients in thin films (DGT) technique has a superior correlation to plant-available P in soils compared to standard chemical extraction tests. In order to identify the plant-available soil P species, we combined DGT with infrared and P K- and $L_{2,3}$-edge X-ray adsorption near-edge structure (XANES) spectroscopy. This was achieved by spectroscopically investigating the dried binding layer of DGT devices after soil deployment. All three spectroscopic methods were able to distinguish between different kinds of phosphates (poly-, trimeta-, pyro- and orthophosphate) on the DGT binding layer. However, infrared spectroscopy was most sensitive to distinguish between different types of adsorbed inorganic and organic phosphates. Furthermore, intermediates of the time-resolved hydrolysis of trimetaphosphate in soil could be analyzed.

1. Introduction

Phosphorus (P) is an essential element for all forms of life. It is necessary for the metabolic process (ADP/ATP) and it is an integral part of the DNA molecule and the cell membrane. Therefore, P is termed a macronutrient and is applied in the form of P-fertilizers in agriculture for crop production.

The plant-availability of soil P can strongly influence the yield of agricultural crops. Hence, several simple chemical extraction methods are used to estimate the plant-available P of soils [1,2]. More recently, several research groups [3-8] have shown that the Diffusive Gradients in Thin films (DGT) technique have a much better correlation to plant-available P in soils than standard chemical extraction tests (e.g. calcium-acetate-lactate (CAL), Colwell, Olsen, water) when soils with different characteristics are considered. The DGT device consists of a binding layer, a diffusion gel and a filter (to protect the gel) assembled in a

plastic holder [8,9]. The dissolved and labile P fraction of the soil from moist soil samples diffuses through the filter and diffusion gel and is subsequently adsorbed to the binding layer during deployment. The amount of adsorbed P on the binding layer, which is the quantity that accounts for the resupply from the solid phase over time, is then used as indicator for P plant-availability of the soil.

Six et al. [6] and Mason et al. [10] discovered by P^{33}/P^{32} labelled P sources that the DGT method accessed the same pool of labile soil P as maize and wheat plants, while conventional P extraction tests also include non-available P pools in their measured quantity. Thus, the soil P compounds which are responsible for high yields of maize and wheat diffused and bound to the DGT binding layer.

The aim of our work was to identify the plant-available P compounds of soils by a novel combination of DGT and spectroscopic techniques. Our approach was to analyze the binding layers of DGT deployed in soils by Fourier Transform infrared (FTIR) spectroscopy, and by K-edge and $L_{2,3}$-edge X-ray adsorption near-edge structure (XANES) spectroscopies. Previously, other groups have shown that X-ray adsorption spectroscopy was able to distinguish between As(III) and As(V) compounds [11] and different mercury compounds [12], respectively, on the DGT binding layer. However, this combination has not been applied to examine highly plant-available P as detected by DGT. Here, we demonstrate the strengths of this approach by i) spectroscopically analyzing DGT deployed in various P solutions (as references), and ii) applying this to a time-resolved investigation of trimetaphosphate (TMP) hydrolysis, a polyphosphate with a high plant-availability [13,14], in incubated P-fertilizer/soil mixtures.

2. Materials and Methods

2.1 DGT experiments

DGT devices [8] (window size: 2.54 cm^2; 0.8 mm APA (polyacrylamide) diffusion layer) with ferrihydrite (Fh; thickness 0.6 mm) and zirconium oxide (ZrO; thickness 0.4 mm) binding layer (DGT Research, Lancaster, UK), respectively, were loaded with 200 mL solutions (50 mg P/L) of various inorganic and organic P compounds (KH_2PO_4, D-glucose-6-phosphate disodium-salt (both Carl Roth, Karlsruhe, Germany), $Ca(H_2PO_4)_2 \cdot H_2O$ (ABCR, Karlsruhe, Germany), $(NH_4)_2HPO_4$ (Merck, Darmstadt, Germany), $Na_4P_2O_7 \cdot 10H_2O$, $Na_5P_3O_{10}$, $(NaPO_3)_3$, adenosine-5´-monophosphate Na-salt (AMP), adenosine-5´-diphosphate Na-salt (ADP), adenosine-5´-triphosphate Na-salt (ATP), adenosine-3´,5´-cyclic monophosphate Na-salt (cAMP), L-α-phosphatidylchinoline, aminomethylphosphonic acid, β-glycerophosphate Na-salt and creatine phosphate (all Alfa Aesar, Karlsruhe, Germany) and phytic acid Na-salt (Sigma-Aldrich, Steinheim, Germany). The DGT devices were deployed for 24 h at 22°C in constantly agitated solutions. After deployment, the binding layers of the DGT devices were dried at room temperature and spectroscopically investigated as described below. Finally, P from the binding layer was eluted with 1 M HNO_3 (for Fh binding layers) or 1 M NaOH (ZrO binding layers) and the P concentration was analyzed by inductively coupled plasma - mass spectroscopy (ICP-MS; Thermo iCAP Q, Dreieich, Germany) to calculate the P mass accumulated to the binding layer.

Furthermore, time-resolved DGT measurements (Fh binding layer) were performed with trimetaphosphate (as sodium salt, $(NaPO_3)_3$) applied to a soil. Therefore, subsoil from a loess-derived brown soil was mixed with quartz sand at 1:1 mass ratio to decrease the P mass fraction (P_{Total}= 180 mg kg^{-1}, P_{CAL} = 10 mg kg^{-1}, pH in 0.01 M $CaCl_2$ = 6.7 of mixture). Sixty grams of soil/sand-mixture was mixed with 6 mg P of TMP (= 100 mg P per kg of soil, as in a previous pot experiment [7,15]) in 100 ml plastic containers. The soil was maintained daily at 60% of the water holding capacity (WHC) at 22°C. DGT was deployed for 24 h at four-time points: at the start of the incubation experiment (0 h) and after 6 hours, 2 and 7 days. Before DGT deployment the water content was increased to 100% WHC.

Additionally, soil samples from a pot experiment [15] with P-fertilizers with novel focus on recycled materials compared to triple super phosphate (TSP) were analyzed. The recycled P materials included sewage sludge from a waste water treatment plant with enhanced biological phosphorus removal (B_{bio}); and sewage sludge precipitated with $FeCl_2$ and post-treated with sodium sulfate under reducing conditions (B_{chem}+Na). These soil samples were taken after the growth experiment. Previous research of these soils showed P DGT results with a superior correlation to the P uptake by maize in the pot experiment [15]. After a 24 h conditioning period of the soils at 60% of the WHC, they were brought to 100% WHC, transferred onto the DGT devices (Fh and ZrO binding layer) and deployed for 24, 48 and 72 h, respectively, at 22°C.

The binding layers from the DGT experiments with the soils from the pot experiment and with the TMP/soil mixture were dried at room temperature and spectroscopically investigated, followed by P extraction with 1 M HNO_3 (Fh) and 1 M NaOH (ZrO), respectively (see above).

2.2 Infrared spectroscopy

Fourier-transform infrared (FT-IR) spectra of the dried DGT binding layers were collected with a Bruker Alpha FT-IR spectrometer (Ettlingen, Germany) with a DTGS detector. The Fh binding layers were measured in transmission mode (spectral resolution 8 cm^{-1}; 32 scans were coadded per spectrum) in a compression cell with diamond windows (Micro Compression Cell II, Thermo Fisher Scientific, Madison, USA). The ZrO binding layers were measured with the eco-attenuated total reflection (ATR) module. The infrared spectra were normalized (Min-Max to 1495-1382 cm^{-1} region) and the peak positions and second derivative analyzed with the software *OPUS* (Bruker, version 7.0).

2.3 P K-edge XANES spectroscopy

P K-edge XANES measurements of dried DGT Fh binding layers were carried out in the High Kinetic Energy Photoelectron Spectrometer (HIKE) endstation [16] located at the BESSY II KMC-1 beamline [17] at Helmholtz-Zentrum Berlin (HZB). The ring was operated in top-up mode at a current of 280 mA. The beamline uses a Si (111) double-crystal monochromator. P K-edge XANES spectra were measured in fluorescence mode using a silicon drift detector XFlash® 4010 (Bruker, Berlin, Germany) from 2130 eV to 2200 eV in steps of 0.25 eV at room temperature. The data was analyzed using the freeware *Demeter Athena* (version 0.9.24) [18]. The spectra were background corrected using a linear regression fit through the pre-edge region [−18 to −8 eV relative to E_0] and a polynomial regression fit through the post-edge region [E_0 +30 to +47 eV].

2.4 P $L_{2,3}$-edge XANES spectroscopy

P $L_{2,3}$-edge XANES analysis of dried DGT Fh binding layers were carried out at the Variable Line Spacing Plane Grating Monochromator (VLS-PGM) beamline [19] at the Canadian Light Source. The electron storage ring was operated in decay mode with a current range of 220-170 mA. All spectra were recorded at room temperature in the energy range from 130 to 155 eV, with a step size of 0.1 eV and a dwell time of 4 s or 16 s. The entrance and exit slits were set to 200 µm. The spectra were collected in total fluorescence yield mode (FLY), using a microchannel plate detector [20] and were normalized with respect to the incident photon flux (I_0). I_0 was simultaneously recorded with the FLY by monitoring the drain current emitted from a Nickel mesh (90% transmission) located in front of the samples. The data were also analyzed using the freeware *Demeter Athena* (version 0.9.24) [18].

3. Results and discussion

3.1 DGT (Fh) of P-solutions

Table 1 shows the P mass accumulated to the Fh binding layer of DGT deployed in solutions containing various P compounds (also relative to KH_2PO_4 (=100%)). The inorganic ortho-, pyro- and polyphosphates show relatively high P adsorption values, best for $Ca(H_2PO_4)_2$ and $Na_4P_2O_7$. In contrast, the values of most organic P compounds (except ADP, ATP and aminomethylphosphonic acid) are much lower, especially for phytic acid and L-α-phosphatidylcholine. This agrees with results of Van Moorleghem et al. [21] and illustrates that the diffusion coefficient for the high molecular weight organic P compounds is lower than for inorganic species. Mohr et al. [22] experimentally determined the diffusion coefficient for AMP (2.9×10^{-6} cm^2 s^{-1}; 20°C) and phytic acid (1.0×10^{-6} cm^2 s^{-1}; 20°C), which is significantly lower than for orthophosphate (5.27×10^{-6} cm^2 s^{-1}; 20°C). Afterwards, these binding layers were used as references for the spectroscopic measurements.

3.2 Spectroscopy of DGT (Fh) binding layers exposed to various P species

Figure 1 shows the normalized FT-IR spectra of the pure Fh binding layer and from the DGT deployed with different P species. In contrast to the blank, the P loaded binding layers show additional absorption bands between 1300 cm^{-1} and 850 cm^{-1}. After subtraction of the pure Fh binding layer spectrum, the absorption bands of the different P compounds adsorbed to the Fh binding layer become clearly visible (Fig. 2 – spectra and second derivative). The orthophosphates show two absorption bands of the P-O stretching vibrations *ca.* 1100 cm^{-1} and 1000 cm^{-1}. This is in agreement to previous studies on sorption of phosphates onto ferrihydrite [23-25]. The pyrophosphate ($Na_4P_2O_7$) shows two additional bands at *ca.* 1160 cm^{-1} and 910 cm^{-1}, the tripolyphosphate ($Na_5P_3O_{10}$) at around 1220 cm^{-1}, 1160 cm^{-1} and 910 cm^{-1} and TMP ($(NaPO_3)_3$) at around 1270 cm^{-1}, 1160 cm^{-1} and a small band *ca.* 910 cm^{-1}. The band at around 910 cm^{-1} is the P-O-P stretching vibration of the condensed phosphates, the band at around 1160 cm^{-1} belongs to the stretching vibration of the PO_3-group and the bands at 1220 cm^{-1} and 1270 cm^{-1} are the stretching vibrations of the

bridging PO_2 [26,27]. The bridging PO_2 stretching vibrations occur for polyphosphates ≥ P_3 only and the frequency of the band is chain length dependent [26].

Additionally, the P K-edge XANES spectra of the Fh binding layers from the DGT experiments with different P solutions were measured. The XANES spectra of the analyzed P standards are very similar (see Fig. 3 top left) and show adsorbed P. A limitation of the P K-edge XANES technique is the inability to reliably distinguish among different phosphate adsorption complexes which result in identical XANES spectra [28]. Furthermore, most iron-P compounds show a minor pre-peak [29], which is not detectable for the Fh binding layers from the DGT experiment. This is probably because of the adsorption complex with Fe, which has only a slight pre-edge feature [28]. However, the zoomed-in edge region and the first derivate of these spectra (Fig. 3 top, middle and right, respectively) show a little shift of the K-edge inflection point ($(NaPO_3)_3$: 2152.5 eV; $Na_4P_2O_7$: 2152.75 eV; and KH_2PO_4: 2153.0 eV). It should be noted that this spectral shift of 0.25 eV is almost similar to the spectral resolution of the beamline (0.2 eV). Thus, FT-IR spectroscopy is much more sensitive to distinguish among different kinds of phosphates absorbed to the Fh binding layer than P K-edge XANES spectroscopy.

In contrast, P $L_{2,3}$-edge XANES spectroscopy provides better resolved spectral features than P K-edge XANES spectroscopy [30]. The features of the P $L_{2,3}$-edge XANES spectra of the Fh binding layers from the DGT experiments with different P solutions come close to the applied poly- and pyrophosphate but with less intensity and are more blurred (see spectra in Fig. 4). The polyphosphate TMP (DGT-$(NaPO_3)_3$) shows two shoulders at around 136.1 eV and 137.1 eV and the pyrophosphate (DGT-$Na_4P_2O_7$) two shoulders at *ca.* 136.5 eV and 137.5 eV. In contrast, the orthophosphate (DGT-KH_2PO_4) absorbed on the DGT Fh binding layer shows no obvious shoulders in the $L_{2,3}$-edge possibly due to more disordered structure compared to standards. Only a slight pre-peak at 136-137 eV was detectable which is characteristic for orthophosphate adsorbed to ferrihydrite [31]. All these phosphates show

characteristic features which could be clearly distinguished from each other. However, it is worth to mention that the sensitivity (fluorescence yields) is much lower for P $L_{2,3}$-edge XANES spectroscopy than for P K-edge XANES spectroscopy, thereby, only Fh binding layers with >43 µg of accumulated P could be analyzed with this technique.

Finally, various organic P compounds on the Fh binding layers were also analyzed by FT-IR spectroscopy (see Fig. S1 and Table 2). The organic orthophosphate monoesters show the P-O stretching vibrations bands around 1080 cm^{-1} and 980 cm^{-1} and the PO_3 stretching vibration at 1160 cm^{-1} in the FT-IR spectra. In comparison to the inorganic orthophosphates the P-O stretching vibrations are shifted (approx. 20 cm^{-1}) to lower wavenumbers. However, it is not possible to differentiate between the different organic orthophosphate monoesters due to the very similar bonding of the phosphate group (R-O-PO_3). In contrast, the organic pyro- and polyphosphate monoesters ADP and ATP show, similarly to the inorganic pyro-/polyphosphates, the P-O-P stretching vibration (926 and 915 cm^{-1}, respectively) and the stretching vibrations of the bridging PO_2 (1216 and 1234 cm^{-1}, respectively) (see Fig. S1; Table 2). ADP shows the bridging PO_2 band, in contrast to the inorganic pyrophosphate, because of the ester bond to the carbon (R-O-PO_2-O-PO_3). Furthermore, this bridging PO_2 band is also detectable for the orthophosphate diesters cAMP (cyclic) and L-α-phosphatidylcholine (linear), respectively, (R-O-PO_2-O-R bond; 1238 cm^{-1} and 1265 cm^{-1}). Additionally, these orthophosphate diesters show also a band at *ca.* 850 cm^{-1}. Moreover, the phosphonates aminomethylphosphonic acid and creatine phosphate show three absorption bands very similar to the orthophosphate monoesters due to the P-O and PO_3-group stretching vibrations of the R-PO_3-group.

3.3 Incubated TMP/soil-mixtures

Figure 5 shows the FT-IR spectra and second derivative of the Fh binding layers from DGT experiments with the incubated TMP/soil-mixtures. At the start of the experiment

absorption bands of ortho-, pyro- and polyphosphates were detected (0 min). Surprisingly, the absorption band of added TMP at 1270 cm^{-1} is not visible. After 6 h of incubation an almost similar spectrum was observed, but after 2 days of incubation the polyphosphate band at around 1220 cm^{-1} is no longer detectable, while the pyrophosphate bands at *ca.* 1160 cm^{-1} and 910 cm^{-1} are still observed. Finally, seven days of incubation led to an almost complete hydrolysis of TMP in the soil to orthophosphates and/or orthophosphate monoesters.

Additionally, P K-edge XANES spectra of the Fh binding layers from the DGT experiments with incubated TMP/soil-mixture were measured (see Fig. 3 bottom). Similar to the XANES spectra of the P standards (Fig. 3 top) the XANES spectra from the incubated TMP/soil-mixture are also very similar. The zoomed-in edge (Fig. 3 bottom middle) and first derivate of these XANES spectra (Fig. 3 bottom right) displays a shift of the edge to higher energy from the beginning of the experiment (0 min. and 6 h) to two and seven days of incubation. These results support the FT-IR data, and together they indicate that TMP is first hydrolyzed in the soil over time to a linear polyphosphate and then to pyro- and orthophosphates, which is in agreement with previous literature [32-34].

The P mass accumulated on the binding layer for the incubation experiment with TMP (see Fig. 5) is very high (40-35 µg P; maximum approx. 58 µg) at the beginning (first day) and rapidly decreased after two days of incubation (9 µg P). However, these amounts of accumulated P on the binding layer were still below the detection limit for P $L_{2,3}$-edge XANES spectroscopy. Based on the FT-IR results of the TMP incubation time series, it is likely that the plant-available P in the incubated TMP/soil-mixture is also decreasing. Previously, Torres-Dorrante et al. [35] showed that the polyphosphate concentration in the soil solution of incubated TMP/soil-mixtures dropped rapidly in the first few days, which is consistent with our findings. Blanchar and Hossner [32] found that TMP, in contrast to other phosphates has a lower sorption rate in soil. Thus, TMP stays in the soil solution and can be easily accessed by DGT. After hydrolysis of the TMP, the orthophosphates can be absorbed to

the soil. This, together with the ageing process of the phosphate, might be an explanation for the high value of accumulated P on the binding layer at the beginning and the decrease after two days of incubation. These experiments were also done with a reduced deployment time for the DGT devices of 3 h (see Fig. S2 in supporting information). However, the results obtained were similar to the 24 h deployment.

3.4 Use of different DGT binding layers

The DGT Fh binding layer can adsorb only up to approximately 58 µg of P and larger amounts of P in fertilizer/soil-mixtures could possibly saturate the binding layer. Therefore, binding layers with higher capacities may be used, such as titanium oxide (TiO_2) [36] or zirconium oxide (ZrO) [37]. DGT experiments showed that the dried TiO_2 binding layers were impossible to analyze by FT-IR spectroscopy because after drying they became stiff and fragile and could not be pressed in the diamond compression cell. The ZrO binding layers were also a bit fragile after drying, but remained sufficiently intact to allow for their analysis by ATR/FT-IR spectroscopy.

Figure 6 shows a comparison of the normalized FT-IR spectra of DGT experiments with ZrO and Fh binding layers, respectively, with different P solutions. In contrast to the Fh binding layer much stronger adsorption bands were detected due to the higher capacity of the ZrO binding layer. Small, adsorbent-dependent shifts in the IR absorption frequencies can be expected since the adsorption process would alter the bond strengths of adsorbing groups (e.g. P-O), similar to the differences observed between pure vs Fh-adsorbed phosphates.

3.5 DGT of soils from pot experiment

Soil from a pot experiment with triple superphosphate [15] was analyzed with different deployment times of the DGT devices (ZrO binding layer). The ATR/FT-IR spectra showed that for all deployment times (24, 48 and 72 h) orthophosphates were adsorbed onto

the ZrO binding layer (see Fig. S3 in the Supporting Information). It is also clear that longer deployment times lead to stronger orthophosphate absorption bands as the adsorbed amount increases.

Analysis of this and other soils from a pot experiment by DGT showed bands from orthophosphates (around 1100 and 1000 cm^{-1}, respectively) and organic orthophosphate monoester (additional band at approx. 1160 cm^{-1}) only on the DGT binding layers (ZrO and Fh; see Fig. S4 and S5, respectively). Notably, the absorption band at 1160 cm^{-1} was also detected for the untreated soil (see Fig. S3 top). Therefore, the orthophosphates appear to originate only from the applied fertilizers. However, the presence of the organic orthophosphate monoester on the binding layer shows that the use of the single orthophosphate diffusion coefficient, as is conventionally used, may not be strictly correct in analyzing DGT P. In this case, (semi-)quantitative P speciation information on the binding layer as demonstrated in this study has the potential to improve the P plant-availability investigations of DGT by allowing the use of multiple diffusion coefficients from the multiple detectable P species.

4. Conclusions

In this paper, we showed the potential for the combination of the DGT technique with spectroscopic methods. Different kinds of phosphates in solutions and soils can be distinguished on the DGT binding layer by infrared and P K- and $L_{2,3}$-edge XANES spectroscopy, respectively (see a summary of all analyzed samples in table S1). However, various orthophosphates adsorbed to the binding layer show very similar FT-IR and XANES spectra, respectively. The organic orthophosphate monoesters also show very similar FT-IR adsorption bands. For the here investigated sample series, the infrared spectra show comparatively more features and thus more information about the adsorbed inorganic and

organic P-species. Additionally, infrared microspectroscopy [38] make it also possible to analyze P compounds on the binding layer with a lateral resolution down to 5 μm^2. Therefore, P species of a spatial soil segment (e.g. rhizosphere) [39] can be mapped and analyzed. Analysis of P hotspots from soil segments could possibly also be done by P $L_{2,3}$-edge XANES microspectroscopy [40] which will be available from autumn of 2019 at the Canadian Light Source. Furthermore, the hydrolysis of TMP in soil shows a further benefit of this combination. Intermediates of the time-resolved hydrolysis were absorbed on the DGT binding layer and could be analyzed afterwards.

Acknowledgments:

CV and DS thank the German Federal Ministry for Food and Agriculture for financial support (2811NA022/2811NA023). CV thanks the German Research Foundation (VO 1794/4-1) for financial support. Collaboration between BAM (CV, CA) and the University of South Australia (RS, EL) was supported by the Australian Technology Network – DAAD Researcher Exchange Scheme (2014). RF acknowledges financial support by the Impuls- und Vernetzungsfonds of the Helmholtz-Association (VH-NG-423). Research described in this paper was performed at the Canadian Light Source, which is supported by the Canada Foundation for Innovation, Natural Sciences and Engineering Research Council of Canada, the University of Saskatchewan, the Government of Saskatchewan, Western Economic Diversification Canada, the National Research Council Canada, and the Canadian Institutes of Health Research. We thank HZB for the allocation of synchrotron radiation beamtime.

References

[1] R. Wuenscher, W. Unterfrauner, R. Peticzka, F. Zehetner, A comparison of 14 soil phosphorus extraction methods applied to 50 agricultural soils from Central Europe. Plant Soil Environ. 61 (2015) 86-96.

[2] M. Yli-Halla, J. Schick, S. Kratz, E. Schnug, Determination of plant available P in soil, in: E. Schnug, L.J. De Kok (Eds.), Phosphorus in agriculture: 100 % zero, Springer, Dordrecht, 2016, pp. 63-93.

[3] N.W. Menzies, B. Kusumo, P.W. Moody, Assessment of P availability in heavily fertilized soils using the diffusive gradient in thin films (DGT) technique. Plant Soil 269 (2005) 1-9.

[4] S. Mason, A. McNeill, M.J. McLaughlin, H. Zhang, Prediction of wheat response to an application of phosphorus under field conditions using diffusive gradients in thin-films (DGT) and extraction methods. Plant Soil 337 (2010) 243-258.

[5] S. Tandy, S. Mundus,J. Yngvesson, T.C. de Bang, E. Lombi, J.K. Schjoerring, S. Husted, The use of DGT for prediction of plant available copper, zinc and phosphorus in agricultural soils. Plant Soil 346 (2011) 167-180.

[6] L. Six, P. Pypers, F. Degryse, E. Smolders, R. Merckx, The performance of DGT versus conventional soil phosphorus tests in tropical soils - An isotope dilution study. Plant Soil 359 (2012) 267-279.

[7] C. Vogel, R. Sekine, D. Steckenmesser, E. Lombi, D. Steffens, C. Adam, Phosphorus availability of sewage sludge-based fertilizers determined by the diffusive gradients in thin films (DGT) technique. J. Plant Nutr. Soil Sci. 180 (2017) 594-601

[8] H. Zhang, W. Davison, R. Gadi, T. Kobayashi, In situ measurement of dissolved phosphorus in natural waters using DGT, Anal. Chim. Acta 370 (1998) 29-38

[9] W. Davison, Diffusive Gradients in Thin-films for environmental measurements, Cambridge University Press, Cambridge, 2016.

[10] S. Mason, M.J. McLaughlin, C. Johnston, A. McNeill, Soil test measures of available P (Colwell, resin and DGT) compared with plant P uptake using isotope dilution. Plant Soil 373 (2013) 711-722.

[11] T. Huynh, H.H. Harris, H. Zhang, B.N. Noller, Measurement of labile arsenic speciation in water and soil using diffusive gradients in thin films (DGT) and X-ray absorption near edge spectroscopy (XANES). Environ. Chem. 12 (2015) 102-111.

[12] A.L. Pham, C. Johnson, D. Manley, H. Hsu-Kim, Influence of sulfide nanoparticles on dissolved mercury and zinc quantification by diffusive gradient in thin-film passive samplers. Environ. Sci. Technol. 49 (2015) 12897−12903.

[13] L.O. Torres-Dorante, N. Claassen, B. Steingrobe, H.W. Olfs, Fertilizer-use efficiency of different inorganic polyphosphate sources: effects on soil P availability and plant P acquisition during early growth of corn. J. Plant Nutr. Soil Sci. 169 (2006) 509-515.

[14] T.M. McBeath, E. Lombi, M.J. McLaughlin, E.K. Bünemann, Polyphosphate-fertilizer solution stability with time, temperature, and pH. J. Plant Nutr. Soil Sci. 170 (2007) 387-391.

[15] D. Steckenmesser, C. Vogel, C. Adam, D. Steffens, Effect of various types of thermochemical processing of sewage sludges on phosphorus speciation, solubility, and fertilization performance. Waste Manage. 62 (2017) 194-203.

[16] M. Gorgoi, S. Svensson, F. Schäfers, G. Öhrwall, M. Mertin, P. Bressler, O. Karis, H. Siegbahn, A. Sandell, H. Rensmo, et al. The high kinetic energy photoelectron spectroscopy facility at BESSY progress and first results. Nucl. Instr. Meth. Phys. Res. A 601 (2009) 48 – 53.

[17] F. Schaefers, M. Mertin, M. Gorgoi, KMC-1: a high resolution and high flux soft x-ray beamline at BESSY. Rev. Sci. Instrum. 78 (2007) 123102.

[18] B. Ravel, M. Newville, ATHENA, ARTEMIS, HEPHAESTUS: data analysis for X-ray absorption spectroscopy using IFEFFIT. J. Synchrotron Radiat. 12 (2005) 537–541.

[19] Y.F. Hu, L. Zuin, G. Wright, R. Igarashi, M. McKibben, T. Wilson, S.Y. Chen, T. Johnson, D. Maxwell, B.W. Yates, T.K. Sham, R. Reininger, Commissioning and performance of the variable line spacing plane grating monochromator beamline at the Canadian Light Source. Rev. Sci. Instrum. 78 (2007) 083109.

[20] M. Kasrai, Z.F. Yin, G.M. Bancroft, K.H. Tan, X-ray fluorescence measurements of XANES at the Si, P and S L-edges. J. Vac. Sci. Technol. A 11 (1993) 2694-2699.

[21] C. Van Moorleghem, L. Six, F. Degryse, E. Smolders, R. Merckx, Effect of organic P forms and P present in inorganic colloids on the determination of dissolved P in environmental samples by the diffusive gradient in thin films technique, ion chromatography, and colorimetry. Anal. Chem. 83 (2011) 5317-5323.

[22] C.W. Mohr, R.D. Vogt, O. Royset, T. Andersen, N.A. Parekh, An in-depth assessment into simultaneous monitoring of dissolved reactive phosphorus (DRP) and low-molecular-weight organic phosphorus (LMWOP) in aquatic environments using diffusive gradients in thin films (DGT). Environ. Sci.: Processes Impacts 17 (2015) 711-727.

[23] M. Nanzyo, Infrared spectra of phosphate sorbed on iron hydroxide gel and the sorption products. Soil Sci. Plant Nutr. 32 (1986) 51-58.

[24] M.I. Tejedor-Tejedor, M.A. Anderson, Protonation of Phosphate on the Surface of Goethite As Studied by CIR-FTIR and Electrophoretic Mobility Langmuir 6 (1990) 602-611.

[25] Y. Arai, D.L. Sparks, ATR–FTIR spectroscopic investigation on phosphate adsorption mechanisms at the ferrihydrite–water interface J. Colloid Interface Sci. 241 (2001) 317-326.

[26] W. Gong, A real time in situ ATR-FTIR spectroscopic study of linear phosphate adsorption on titania surfaces. Int. J. Miner. Process. 63 (2001) 147-165.

[27] X.H. Guan, Q. Liu, G.H. Chen, C. Shang, Surface complexation of condensed phosphate to aluminum hydroxide: An ATR-FTIR spectroscopic investigation *J.* Colloid Interface Sci. 289 (2005) 319-327.

[28] J.G. Hamilton, G. Hilger, D.J. Peak, Mechanisms of tripolyphosphate adsorption and hydrolysis on goethite. Colloid Interface Sci. 491 (2017) 190–198.

[29] N. Khare, D. Hesterberg, J.D. Martin, XANES investigation of phosphate sorption in single and binary systems of iron and aluminum oxide minerals. Environ. Sci. Technol. 39 (2005) 2152-2160.

[30] J. Kruse, P. Leinweber, K.W. Eckhardt, F. Godlinski, Y. Hu, L. Zuin, Phosphorus $L_{2,3}$-edge XANES: overview of reference compounds. J. Synchrotron Radiat. 16 (2009) 247-259.

[31] W. Xiong, J. Peng, Y. Hu, Use of X-ray adsorption near edge structure (XANES) to identify physiorption and chemisorption of phosphate onto ferrihydrite-modified diatomite. J. Colloid Interface Sci. 368 (2012) 528-532.

[32] R.W. Blanchar, L.R. Hossner, Hydrolysis and sorption reactions of orthophosphate, pyrophosphate, tripolyphosphate, and trimetaphosphate anions added to an Elliot soil. Soil Sci. Soc. Amer. Proc. 33 (1969) 141-144.

[33] L.M. Busman, M.A. Tabatabai, Hydrolysis of trimetaphosphate in soils. Soil Sci. Soc. Amer. Proc. 49 (1985) 630-636.

[34] R.P. Dick, M.A. Tabatabi, Factors affecting hydrolysis of polyphosphates in soils. Soil Sci. 143 (1987) 97-104.

[35] L.O. Torres-Dorante, N. Claassen, B. Steingrobe, H.W. Olfs, Hydrolysis rates of inorganic polyphosphates in aqueous solution as well as in soils and effects on P availability. J. Plant Nutr. Soil Sci. 168 (2005) 352-358.

[36] J.G. Panther, P.R. Teasdale, W.W. Bennett, D.T. Welsh, H. Zhao, Titanium dioxide-based DGT technique for in situ measurement of dissolved reactive phosphorus in fresh and marine waters. Environ. Sci. Technol. 44 (2010) 9419-9424

[37] S. Ding, D. Xu, Q. Sun, H. Yin, C. Zhang, Measurement of dissolved reactive phosphorus using the diffusive gradient in thin films technique with a high-capacity binding phase. Environ. Sci. Technol. 44 (2010) 8169-8174.

[38] E. Grotheer, C. Vogel, O. Kolomiets, U. Hoffmann, M. Unger, H.W. Siesler, FT-IR and NIR spectroscopic imaging: Principles, practical aspects, and applications in Material and pharmaceutical science, in: R. Salzer, H.W. Siesler (Eds.), Infrared and Raman Spectroscopic Imaging, 2nd Edition, Wiley-VCH, Weinheim, 2014, pp. 341-396.

[39] A. Kreuzeder, J. Santner, T. Prohaska, W.W. Wenzel, Gel for simultaneous chemical imaging of anionic and cationic solutes using diffusive gradients in thin films. Anal. Chem. 85 (2013) 12028−12036.

[40] C. Vogel, C. Rivard, I. Tanabe, C. Adam, Microspectroscopy – Promising technique to characterize phosphorus in soil. Comm. Soil Sci. Plant Anal. 47 (2016) 2088-2102.

Table and Figure Caption:

Table 1: DGT-measurable P over 24 h to the Fh binding layer of DGT devices from P-solutions (50 mg P/L) of various P compounds

Table 2: Detected IR absorption bands (cm^{-1}) of various inorganic and organic P compounds adsorbed to the Fh binding layer. (*v* = streching vibration**)**

Figure 1: FT-IR spectra of Fh binding layers from DGT experiments with solutions of different phosphates

Figure 2: Blank subtracted FT-IR spectra (left) and second derivative (right) of Fh binding layers from DGT experiments with solutions of different inorganic phosphates

Figure 3: P K-edge XANES spectra of Fh binding layers from DGT experiments with solutions of different phosphates (top left) and time-resolved incubated TMP in soil (below left), zoomed in edge-region (middle) and their first derivative of the related edge region (right); the vertical lines show the edge and first derivative of the edge for the polyphosphate (blue), pyrophosphate (green) and orthophosphate (red).

Figure 4: P $L_{2,3}$-edge XANES spectra of Fh binding layers from DGT experiments with solutions of different phosphates in comparison to spectra of the applied phosphates

Figure 5: Blank subtracted FT-IR spectra (left) and second derivative (right) of Fh binding layers from DGT experiments of time-resolved incubated TMP in soil

Figure 6: Comparison between FT-IR spectra of ZrO (black) and Fh (red) binding layers from DGT experiments with solutions of different phosphates

Table 1:

	phosphate type	molecular weight	P mass accumulated to binding layer	Accumulated P relative to KH_2PO_4
KH_2PO_4	orthophosphate	136 g/mol	58.5 ± 0.4 µg	100% ± 1%
$Ca(H_2PO_4)_2$	orthophosphate	252 g/mol	58.5 ± 4.7 µg	100% ± 8%
$Na_4P_2O_7$	pyrophosphate	266 g/mol	49.7 ± 5.3 µg	85% ± 9%
$Na_5P_3O_{10}$	polyphosphate	368 g/mol	34.5 ± 0.6 µg	59% ± 1%
$(NaPO_3)_3$	polyphosphate	306 g/mol	43.3 ± 4.7 µg	74% ± 8%
β-Glycero phosphate	orthophosphate monoester	216 g/mol	29.8 ± 2.9 µg	51% ± 5%
Phytic acid	orthophosphate monoester	660 g/mol	6.4 ± 0.6 µg	11% ± 1%
Glucose-6-phosphate	orthophosphate monoester	308 g/mol	29.3 ± 4.7 µg	50% ± 8%
AMP	orthophosphate monoester	391 g/mol	31.6 ± 0.6 µg	54% ± 1%
ADP	pyrophosphate monoester	471 g/mol	48.6 ± 1.2 µg	83% ± 2%
ATP	polyphosphate monoester	533 g/mol	69.6 ± 0.8 µg	119% ± 2%
cAMP	cyclic phosphate diester	351 g/mol	10.5 ± 4.1 µg	18% ± 7%
L-α-Phosphatidylcholine	phosphate diester	644 g/mol	2.9 ± 0.5 µg	5% ± 1%
Aminomethylphosphonic acid	phosphonate	111 g/mol	47.4 ± 1.2 µg	81% ± 2%
Creatine phosphate	phosphonate	263 g/mol	23.4 ± 2.3 µg	40% ± 4%

Table 2:

	νPO_2 bridging	νPO_3	ν_1P-O	ν_2P-O	ν(P-O-P)	ν(O-P-O) diester
Inorg. orthophosphate			1087	1000		
Inorg. pyrophosphate		1159	1088	1019	910	
Inorg. tripolyphosphate	1220	1161	1084	978	906	
Inorg. trimetaphosphate	1270	1158	1087	988	903	
AMP		1153	1079	981		
cAMP	1238	1159	1068	1010	909	849
ADP	1216	1161	1088	1001	926	
ATP	1234	1164	1087	989	915	
β-Glycero phosphate		1155	1070	976		
Phytic acid		1166	1070	984		
Glucose-6-phosphate		1153	1082	981		
L-α-Phosphatidylcholine	1267	1160		1003		854
Aminomethylphosphonic acid		1132	1053	985		
Creatine phosphate		1158	1095	979		

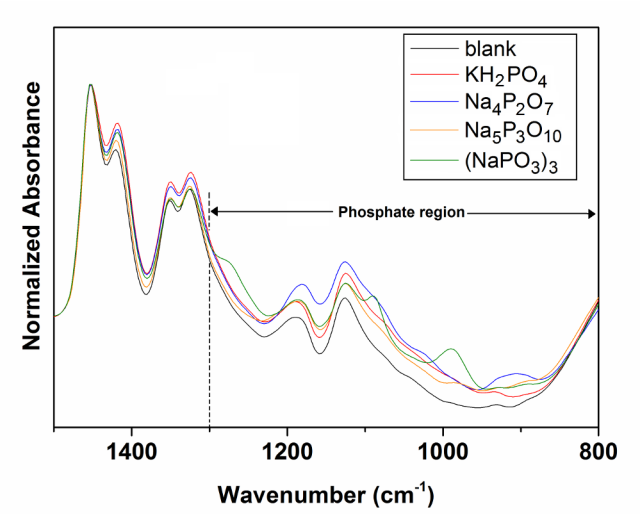

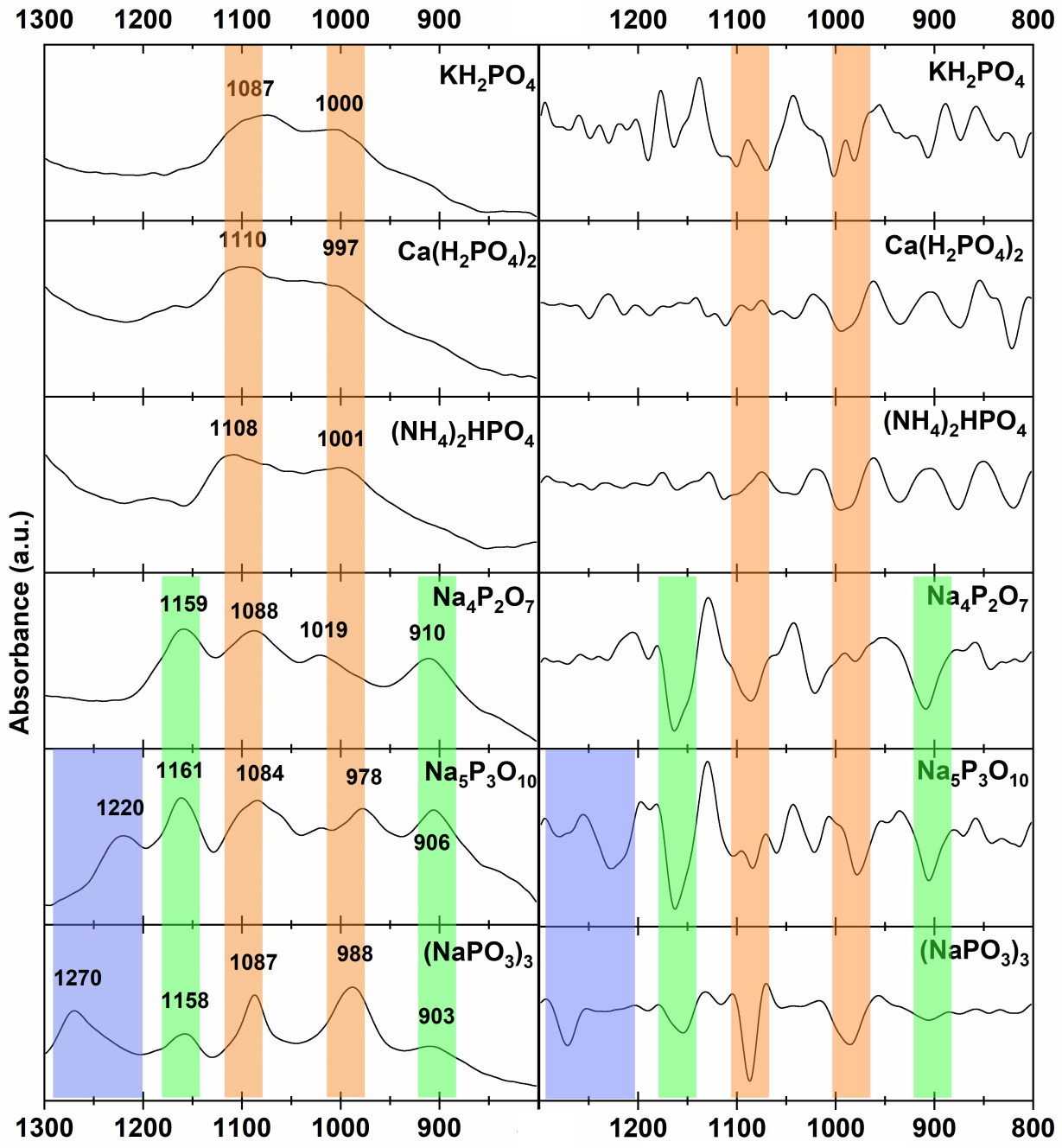
1300
1200
1100
1000
900
800
Absorbance (a.u.)
KH2PO4
1087
1000
Ca(H2PO4)2
1110
997
(NH4)2HPO4
1108
1001
Na4P2O7
1159
1088
1019
910
Na5P3O10
1220
1161
1084
978
906
(NaPO3)3
1270
1158
1087
988
903

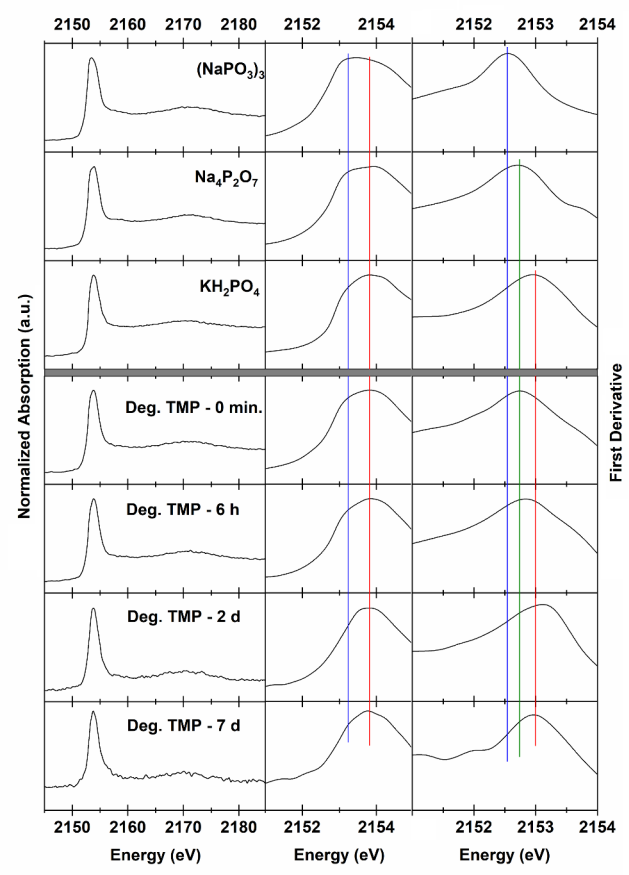

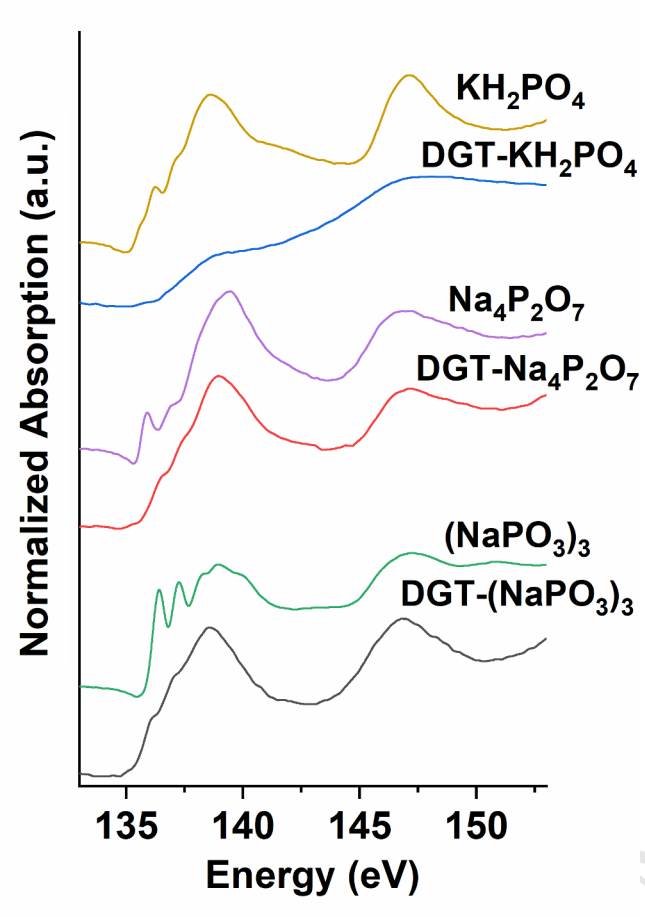

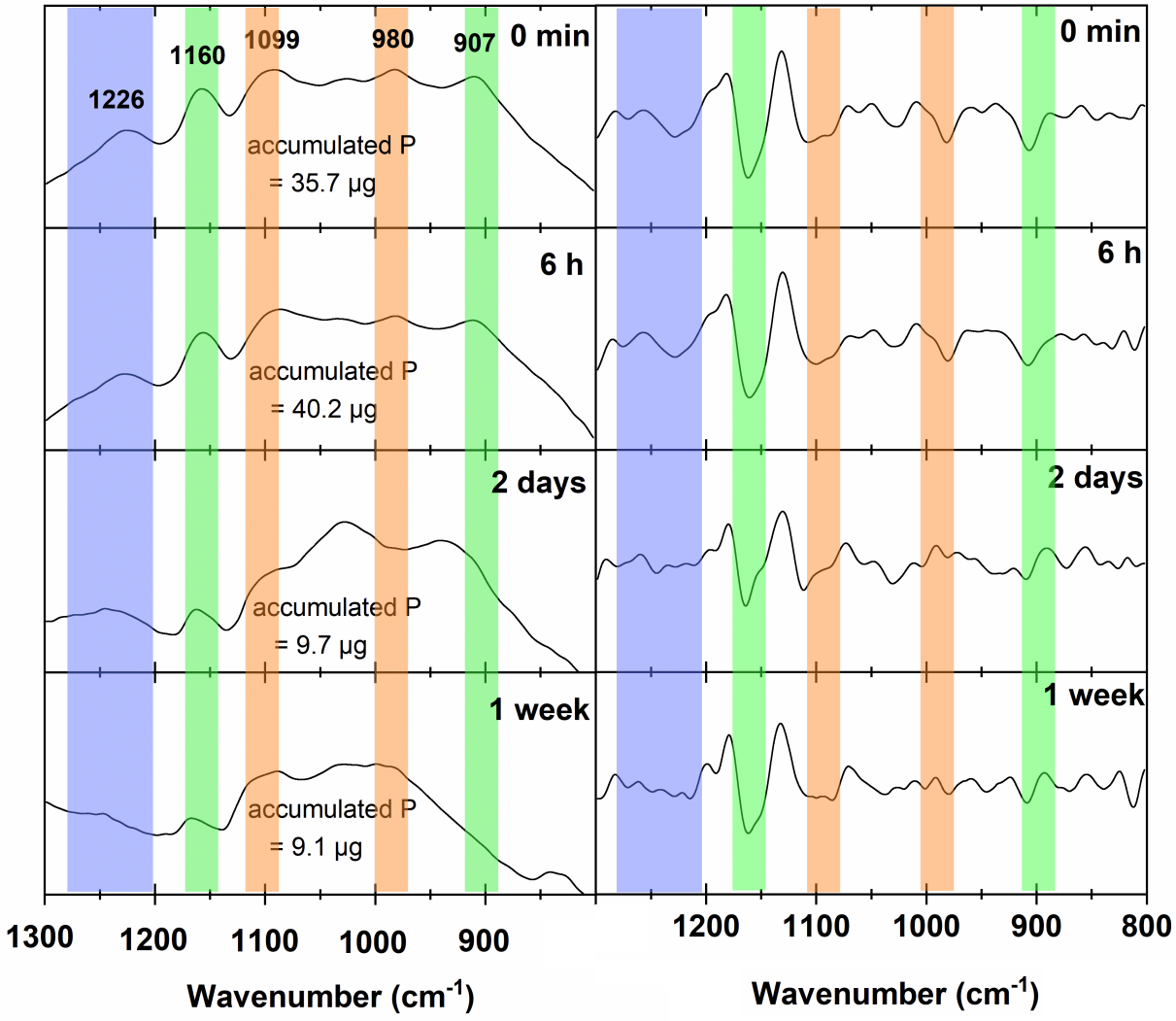
1226
1160
1099
980
907
0 min
accumulated P
= 35.7 µg
6 h
accumulated P
= 40.2 µg
2 days
accumulated P
= 9.7 µg
1 week
accumulated P
= 9.1 µg
1300
1200
1100
1000
900
Wavenumber (cm-1)
0 min
6 h
2 days
1 week
1200
1100
1000
900
800
Wavenumber (cm-1)

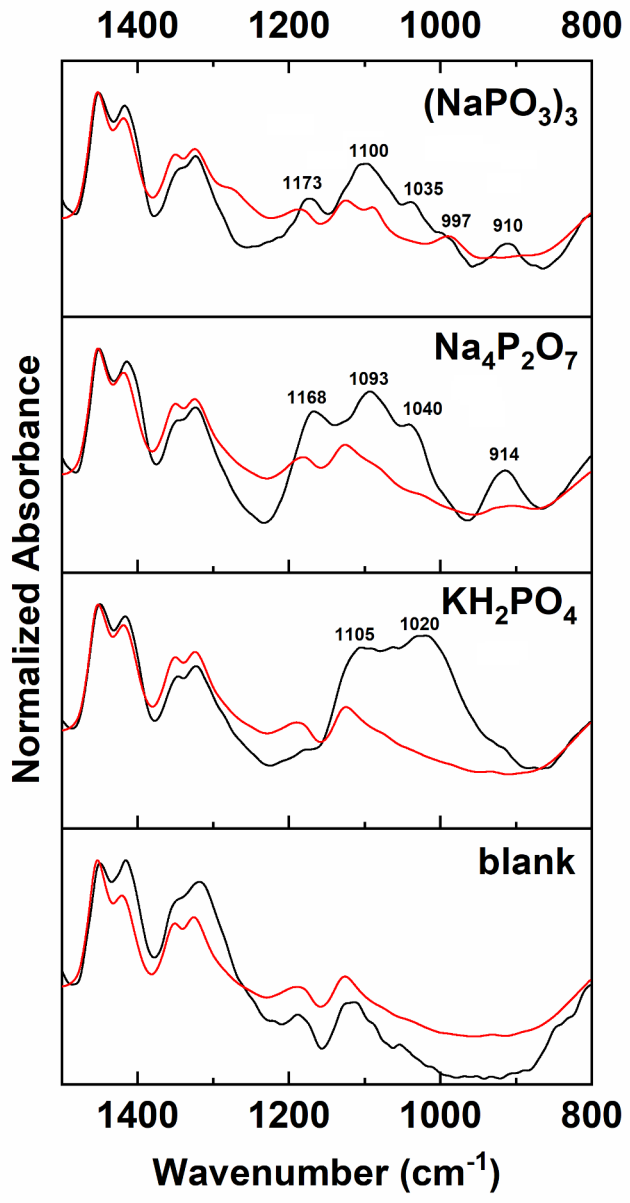

Highlights:

- Combination of DGT and spectroscopic techniques determines plant-available phosphorus species in soils
- Intermediates of time-resolved soil phosphorus reactions can be analyzed
- Spectroscopic mapping techniques can detect phosphorus species of a spatial soil segment

Declarations of interest: none